

GeV Scale Inelastic Dark Matter with Dark Photon Mediator via Direct Detection and Cosmological/Laboratory Constraints

HONG-JIAN HE,^{1,2,3,*} YU-CHEN WANG,^{2,†} and JIAMING ZHENG^{1,‡}

¹*Tsung-Dao Lee Institute & School of Physics and Astronomy,
Key Laboratory for Particle Astrophysics and Cosmology (MOE),
Shanghai Key Laboratory for Particle Physics and Cosmology,
Shanghai Jiao Tong University, Shanghai 200240, China*

²*Institute of Modern Physics & Physics Department, Tsinghua University, Beijing 100084, China*

³*Center for High Energy Physics, Peking University, Beijing 100871, China*

We propose a new candidate of GeV scale inelastic dark matter (DM), which can be either scalars or fermions. Both the DM and the right-handed first family fermions join interactions of a dark $U(1)_X$ gauge group. Our construction is highly testable and receives nontrivial experimental constraints. We study the scattering rate of light DM with electrons in the XENON1T experiment and with nucleons in the XENON1T, CRESST-III, CDEX-1B and DarkSide-50 experiments. We resolve the recent XENON1T anomaly via electron recoil detection. Combining the XENON1T constraints from both electron recoils and nucleon recoils (including Migdal effect), we predict the inelastic DM mass $\lesssim 1$ GeV. We further analyze the limits by the DM relic abundance, the lifetime of the heavier DM component, the collider searches, and the electroweak precision tests, with which we identify the viable parameter space of the GeV scale inelastic DM. [arXiv:2012.05891]

I. Introduction

Searching for GeV scale light dark matter (DM) particles is a very challenging task because the conventional direct detection via DM-nucleon recoil becomes hard for DM mass $\lesssim 5$ GeV. Hence, measuring the DM-electron recoil spectrum has provided an important means for the light DM direct detection. The XENON collaboration [1] recently announced a 3.5σ excess of events with low electron recoil energy in its Science Run-I [2]. The XENON1T detector recorded 285 events for the recoil energy $E_R = (1-7)$ keV, among which the expected background events are 232 ± 15 [2]. This excess centers around $E_R = (2-3.5)$ keV. Lately, the PandaX-II collaboration also reported an independent DM search by measuring the low energy electron recoil spectrum with robust estimates of backgrounds [3]. It is consistent with the XENON1T measurement [2] although its sensitivity is not yet enough to either confirm or exclude the DM interpretation of the XENON1T anomaly. There have been possible explanations for this excess in the literature, including unexpected Tritium background [2, 4] and various new physics models [5-8].

One attractive resolution of the XENON1T anomaly is the exothermic inelastic scattering [7, 8] between the DM and electron. In this scenario, the DM consists of two components (X, X') with a small mass-splitting $\Delta m \equiv m_{X'} - m_X$, which is around the anomalous recoil energy region (2-3) keV of XENON1T. The heavier DM component X' is cosmologically stable because its decay to the lighter DM component X can be highly suppressed by

the small mass-splitting Δm . Inside the xenon detector, X' scatters inelastically with the xenon electron and deexcite to X . The DM mass-splitting manifests itself as a peak in the electron recoil energy spectrum. On the other hand, the recoil energy from the elastic DM-electron scattering is too small to be detectable in XENON1T unless the DM particles are very fast moving [5]. To realize the XENON1T anomaly, we can estimate the required normalized cross section of the DM-electron inelastic scattering, $\bar{\sigma}_e/m_X \approx 8.8 \times 10^{-44} \text{cm}^2/\text{GeV}$, by considering the DM (X, X') of equal amount and the DM-electron interaction of scalar or vector type [8]. Here we define $\bar{\sigma}_e \equiv \sigma_{Xe}(|\mathbf{q}|=0)$ as the scattering cross section of $X'e^- \rightarrow Xe^-$ in the zero-momentum-exchange limit $|\mathbf{q}|=0$.

In the literature, the exothermic inelastic scattering mostly arise from exchanging a light dark photon with couplings to leptons by assuming a tiny kinetic mixing between the dark photon and the standard model (SM) photon [7]. These models require a large hierarchy between the dark photon-lepton coupling and the dark photon-DM coupling. So the dark photons could be hidden from various collider searches by tuning the kinetic mixing of the dark photon with photon down to $O(10^{-3}-10^{-6})$. The origin of such tiny kinetic mixing remains obscure [9], so we will not pursue this for the current study.

In this work, we propose an anomaly-free and renormalizable inelastic DM model in which the DM and the right-handed first family fermions join the interactions of a dark $U(1)_X$ gauge group. We achieve the desired $O(\text{keV})$ mass-splitting of the inelastic DM by a scalar seesaw mechanism without fine-tuning. We show that this model is viable for the inelastic DM of mass $\lesssim 1$ GeV, which can provide the observed anomaly in the XENON1T electron recoil spectrum [2] and be consistent

*hjhe@sjtu.edu.cn; hjhe@tsinghua.edu.cn

†wang-yc15@mails.tsinghua.edu.cn

‡zhengjm3@sjtu.edu.cn

Group	Q_{L1}	u_R	d_R	L_1	e_R	ν_{R1}	H_1	H_2	S	S'	ϕ	\widehat{X}	$\widehat{\chi}$
$SU(2)_L$	2	1	1	2	1	1	2	2	1	1	1	1	1
$U(1)_Y$	$\frac{1}{6}$	$\frac{2}{3}$	$-\frac{1}{3}$	$-\frac{1}{2}$	-1	0	$\frac{1}{2}$	$\frac{1}{2}$	0	0	0	0	0
$U(1)_X$	0	$\frac{1}{2}$	$-\frac{1}{2}$	0	$-\frac{1}{2}$	$\frac{1}{2}$	$\frac{1}{2}$	0	-1	$\frac{1}{2}$	-3	3	$\frac{3}{2}$
\mathbb{Z}_2	$+$	$+$	$+$	$+$	$+$	$+$	$+$	$+$	$+$	$+$	$+$	$-$	$-$

TABLE I: Particle content and group assignments of the present model. Here Q_{L_j} and L_j denote the left-handed weak doublet of the SM quarks and leptons, respectively, and the subscript j is the fermion family index of the SM. The second column from right defines the scalar inelastic DM \widehat{X} (Sec. II A), while the last column defines the fermionic inelastic DM $\widehat{\chi}$ (Sec. II B).

with the DM-nucleon recoil detections (of low threshold) by XENON1T [13], CRESST-III [16], CDEX-1B [15], and DarkSide-50 [14] experiments. For the dark photon mediator with mass $\lesssim 1.5$ GeV, this model can provide the observed DM relic abundance and ensure the heavier DM component cosmologically stable. Since the mediator couples to the right-handed electrons, we derive non-trivial constraints by various laboratory measurements, including the electroweak precision tests and collider searches.

This paper is organized as follows. We construct our model in Sec. II. Then, in Sec. III we analyze the DM-electron and DM-nucleon recoil signals in various direct detection experiments. In Sec. IV, we study the cosmological constraints on our model, including the X' lifetime and the DM relic density. In Sec. V, we study other laboratory constraints, including the electroweak precision tests and the collider searches. Finally, we conclude in Sec. VI. Appendix A elaborates our analysis of the Higgs sector in this model.

II. Inelastic DM with Dark Photon Mediator

To realize the DM-electron interaction, we make a minimal extension of the SM by a dark $U(1)_X$ gauge group under which both the DM and the right-handed first family fermions are charged. We also include three right-handed Majorana neutrinos ν_{Rj} ($j = 1, 2, 3$). We denote the $U(1)_X$ gauge boson (dark photon) by A'_μ . The Higgs sector consists of two Higgs doublets plus three singlet scalars S , S' and ϕ , charged under $U(1)_X$. The electroweak symmetry breaking is realized by two Higgs doublets H_1 and H_2 with vacuum expectation values (VEVs) $\langle H_j \rangle = (0, v_j)^T$ and the combined VEV is $v_h = \sqrt{v_1^2 + v_2^2} \simeq 174$ GeV. We will set $v_1^2 \ll v_2^2$, so the observed 125 GeV Higgs boson is mostly made of the CP even neutral component of H_2 . The dark $U(1)_X$ gauge group is mainly broken by the VEVs of the singlet scalars S and S' , whose VEVs $\langle S \rangle = v_S$ and $\langle S' \rangle = v_{S'}$ are of $O(100)$ GeV. Our model sets the first family fermions charged under $U(1)_X$, and the second and third fam-

ily fermions as $U(1)_X$ singlets. In the following, we will study the case of scalar DM $\widehat{X} = (X + iX')/\sqrt{2}$ and the case of fermionic DM $\widehat{\chi} = (\chi_1, \chi_2^\dagger)^T$, respectively. In Table I, we summarize the particle content and charge assignments of our model for the dark sector, the Higgs sector, and the first family fermions.

A. Inelastic Scalar DM with Dark $U(1)_X$

The DM particles (X, X') form a complex scalar $\widehat{X} = (X + iX')/\sqrt{2}$ with $U(1)_X$ charge $q_{\widehat{X}}$. As we will show, the spontaneous breaking of $U(1)_X$ can generate the desired mass-splitting Δm between X and X' . Our model sets the left-handed fermion doublets as $U(1)_X$ singlets. This forbids the decay channel $X' \rightarrow X\bar{\nu}\nu$, and thus ensures that the current DM relic abundance consists of about equal amounts of (X, X') so far. The anomaly cancellation conditions then uniquely determine the $U(1)_X$ charges of the first family fermions up to an overall normalization factor. Here the flavor non-universality of $U(1)_X$ is to maintain the X' lifetime being longer than the age of our universe, as will be shown in Sec. IV.

We write down the relevant Lagrangian terms of the DM sector as follows:

$$\Delta\mathcal{L}_{\text{DM}} \supset |D^\mu\widehat{X}|^2 - m_{\widehat{X}}^2|\widehat{X}|^2 - \lambda_X|\widehat{X}|^4 - (\lambda_{X\phi}\widehat{X}^2\phi^2 + \text{h.c.}) - \sum_i \lambda_{X\psi_i}|\widehat{X}|^2|\psi_i|^2, \quad (1)$$

where the scalar fields $\psi_i = H_1, H_2, S, S', \phi$. Due to the $U(1)_X$ charge assignments, the right-handed SM fermions in the first family only couple to H_1 , while the second and third families of right-handed fermions only interact with H_2 . Thus, we can write down the Lagrangian including the relevant Yukawa terms with ν_{Rj} and the relevant potential terms with scalar singlets:

$$\Delta\mathcal{L} \supset \bar{e}_R i \not{D} e_R - \sum_{i=1}^3 \left(y_{i1}^\nu \bar{L}_i \tilde{H}_1 \nu_{R1} + \sum_{j=2}^3 y_{ij}^\nu \bar{L}_i \tilde{H}_2 \nu_{Rj} + \text{h.c.} \right) - \frac{1}{2} \left(y_S \nu_{R1}^T S \nu_{R1} + \sum_{i,j=2}^3 M_{Rij} \nu_{Ri}^T \nu_{Rj} + \text{h.c.} \right) + M_S^2 |S|^2 + M_{S'}^2 |S'|^2 + (M'_{12} H_1^\dagger H_2 S' + \text{h.c.}) - M_\phi^2 |\phi|^2 + (\lambda_{S\phi} S^3 \phi^* + \text{h.c.}). \quad (2)$$

We note that the cubic term $M'_{12} H_1^\dagger H_2 S'$ can ensure the pseudoscalars to be massive. In Eq. (2), the squared masses ($M_S^2, M_{S'}^2, M_\phi^2$) are all positive, so S and S' acquire VEVs from their potentials directly, whereas ϕ can only obtain a small VEV induced from $\langle S \rangle$ and $\langle S' \rangle$. In our model, the scalar potential holds CP conservation, under which all the scalar couplings and VEVs are real. Eq. (2) shows that the singlet S and the right-handed neutrino ν_{R1} form a Yukawa interaction which generates a weak scale Majorana mass $M_{R1} = y_{S1} v_S$ for ν_{R1} . The second and third family right-handed neutrinos are $U(1)_X$ singlets, so they directly form Majorana mass

terms. Thus, the light neutrino masses are generated by the type-I seesaw mechanism.

From the Lagrangian (1), we see that the DM mass is determined by the DM quadratic mass term and the DM couplings to $|H_i|^2$, $|S|^2$ and $|S'|^2$. The mass-splitting between the two DM components is determined by the unique quartic interaction $\widehat{X}^2\phi^2$, where the singlet VEV $\langle\phi\rangle$ is naturally small as generated by a scalar seesaw from the potential terms in the last line of Eq.(2). This is because ϕ is much heavier than all the other scalars and leads to $v_\phi \equiv \langle\phi\rangle \simeq \lambda_{S\phi}v_S^3/M_\phi^2$. Thus, we derive the (X, X') mass-splitting:

$$\frac{m_{X'} - m_X}{m_X} \simeq \frac{\lambda_{X\phi}v_\phi^2}{m_X^2} = \frac{2\lambda_{X\phi}\lambda_{S\phi}^2v_S^6}{m_X^2M_\phi^4}. \quad (3)$$

Hence, to realize the desired $O(\text{keV})$ mass-splitting for explaining the XENON1T anomaly, we can choose the sample inputs without fine-tuning, $\lambda_{X\phi}, \lambda_{S\phi} = O(0.01)$, $v_S = O(100)$ GeV, $m_X = O(\text{GeV})$, and $M_\phi = O(\text{TeV})$.

Since the Higgs doublet H_1 carries charges of both $U(1)_Y$ and $U(1)_X$, its VEV induces mass-mixing between their gauge bosons. Denoting the neutral gauge bosons of $SU(2)_L$, $U(1)_Y$ and $U(1)_X$ as $(W_\mu^3, B_\mu, \mathcal{X}_\mu)$, we derive their mass-eigenstates (Z_μ, A_μ, A'_μ) to the leading order of the gauge coupling $g_X \ll 1$ and VEV ratio $v_1^2/v_h^2 \ll 1$, with the mass-eigenvalues,

$$\begin{aligned} m_A^2 &= 0, \\ m_{A'}^2 &\simeq 2g_X^2 \left(v_S^2 + \frac{1}{4}v_{S'}^2 \right), \\ M_Z^2 &\simeq \frac{1}{2} \left(g^2 + g'^2 + g_X^2 \frac{v_1^4}{v_h^4} \right) v_h^2, \end{aligned} \quad (4)$$

and their leading order mixing matrix,

$$\begin{pmatrix} A'_\mu \\ A_\mu \\ Z_\mu \end{pmatrix} = \begin{pmatrix} 1 & \frac{-g'g_X}{g^2+g'^2} \frac{v_1^2}{v_h^2} & \frac{gg_X}{g^2+g'^2} \frac{v_1^2}{v_h^2} \\ 0 & \frac{g}{\sqrt{g^2+g'^2}} & \frac{g'}{\sqrt{g^2+g'^2}} \\ \frac{-g_X}{\sqrt{g^2+g'^2}} \frac{v_1^2}{v_h^2} & \frac{-g'}{\sqrt{g^2+g'^2}} & \frac{g}{\sqrt{g^2+g'^2}} \end{pmatrix} \begin{pmatrix} \mathcal{X}_\mu \\ B_\mu \\ W_\mu^3 \end{pmatrix}. \quad (5)$$

B. Inelastic Fermionic DM with Dark $U(1)_X$

The mechanism of realizing $O(\text{keV})$ mass-splitting for the scalar inelastic DM in Sec. II A can be extended to the case of inelastic fermionic DM. In this subsection, we present a construction of inelastic fermionic DM. In this model, the charge assignments (Table I) and the scalar potential (2) remain the same as before, except the fermionic DM $\widehat{\chi}$ has a different $U(1)_X$ charge as shown in the last column of Table I. The fermionic DM contains two Weyl spinors χ_1 and χ_2 , with opposite $U(1)_X$ charges $q_{\chi_1} = -q_{\chi_2} = \frac{3}{2}$. They can form a Dirac spinor $\widehat{\chi} = (\chi_1, \chi_2^\dagger)^T$, which is vector-like under $U(1)_X$. Thus, the dark sector contains the following gauge-invariant Lagrangian terms:

$$\Delta\mathcal{L} \supset \chi_1^\dagger \mathbf{i}\bar{\sigma}^\mu D_\mu \chi_1 + \chi_2^\dagger \mathbf{i}\bar{\sigma}^\mu D_\mu \chi_2 - (m_{\widehat{\chi}}\chi_1\chi_2 + \text{h.c.})$$

$$+ (y_{\phi\chi_1}\chi_1\chi_1\phi + y_{\phi\chi_2}\chi_2\chi_2\phi^* + \text{h.c.}), \quad (6)$$

where the parameters $(m_{\widehat{\chi}}, y_{\phi\chi_1}, y_{\phi\chi_2})$ are positive after proper phase rotations of (ϕ, χ_1, χ_2) . As shown in Sec. II A, the scalar field ϕ acquires a small VEV $v_\phi \simeq \lambda_{S\phi}v_S^3/M_\phi^2$ due to the scalar seesaw from Eq.(2). The VEV v_ϕ will induce additional Majorana masses for (χ_1, χ_2) through the Yukawa interactions in Eq.(6). Thus, we have the following DM mass terms:

$$\mathcal{L}_{\chi_1\chi_2} \supset -m_{\widehat{\chi}}\chi_1\chi_2 + \delta m_1\chi_1\chi_1 + \delta m_2\chi_2\chi_2 + \text{h.c.}, \quad (7)$$

where $(\delta m_1, \delta m_2) = (y_{\phi\chi_1}v_\phi, y_{\phi\chi_2}v_\phi)$. To rotate (χ_1, χ_2) into the mass-eigenstates (χ, χ') , we make the following decomposition:

$$\chi_1 \simeq \frac{1}{\sqrt{2}}(\chi - \mathbf{i}\chi'), \quad \chi_2 \simeq \frac{1}{\sqrt{2}}(\chi + \mathbf{i}\chi'). \quad (8)$$

In the limit $v_\phi \ll m_{\widehat{\chi}}$, we derive the following Majorana masses for the DM mass-eigenstates (χ, χ') :

$$\begin{aligned} m_\chi &\simeq m_{\widehat{\chi}} - (\delta m_1 + \delta m_2), \\ m_{\chi'} &\simeq m_{\widehat{\chi}} + (\delta m_1 + \delta m_2), \end{aligned} \quad (9)$$

which have a mass-splitting,

$$\Delta m_\chi \simeq 2(\delta m_1 + \delta m_2). \quad (10)$$

To realize the required mass-splitting of $O(\text{keV})$ for explaining the XENON1T anomaly, we choose the natural sample inputs, $\lambda_{S\phi}, y_{\phi\chi_1}, y_{\phi\chi_2} = O(0.01)$, $v_S = O(20)$ GeV, and $M_\phi = O(\text{TeV})$. With these, we deduce a small VEV $v_\phi = O(0.1)$ MeV and thus the desired mass-splitting $\Delta m_\chi = O(\text{keV})$. From Eq.(6), we deduce the $U(1)_X$ gauge interactions for the DM fields (χ, χ') :

$$\mathcal{L}_{\text{int}} \supset \mathbf{i}q_{\widehat{\chi}}g_X(\chi^\dagger\bar{\sigma}_\mu\chi' - \chi'^\dagger\bar{\sigma}_\mu\chi)\mathcal{X}^\mu. \quad (11)$$

We note that the diagonal vertices $\chi\text{-}\chi\text{-}\mathcal{X}^\mu$ and $\chi'\text{-}\chi'\text{-}\mathcal{X}^\mu$ vanish, whereas the above non-diagonal vertices can induce the desired inelastic scattering for explaining the XENON1T anomaly of DM-electron recoils.

Most discussions in the rest of this paper can apply to both the scalar and fermionic DM. For the simplicity of notations, unless specified otherwise, we will use the same symbols $(\Delta m, m_X)$ and (\widehat{X}, X, X') for both scalar and fermionic DM. For the fermionic DM, these notations refer to $(\Delta m_\chi, m_{\widehat{\chi}})$ and $(\widehat{\chi}, \chi, \chi')$.

III. Analyzing Constraints of DM Direct Detections

For the present models, we derive the DM-electron inelastic scattering cross section with zero-momentum-transfer, which holds for both the scalar DM and fermionic DM:

$$\bar{\sigma}_e \equiv \sigma_{Xe}(|\mathbf{q}|=0) = \frac{q_e^2 q_{\text{DM}}^2 g_X^4}{4\pi} \frac{m_e^2}{m_A^4}, \quad (12)$$

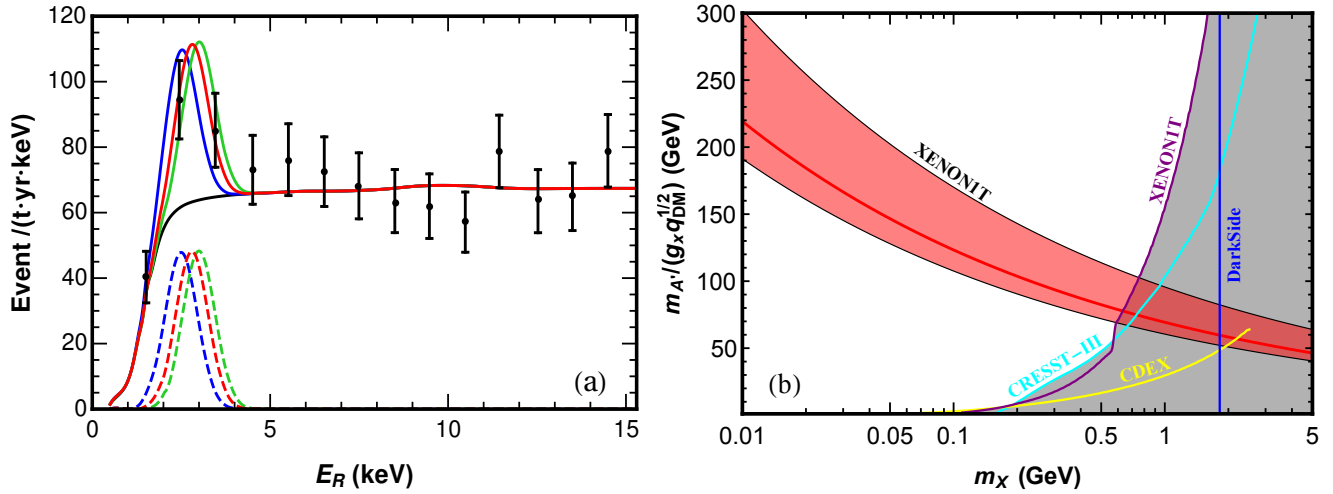


FIG. 1: Plot (a): Electron recoil energy spectrum as predicted by the inelastic DM and measured by XENON1T [2]. The (green, red, blue) dashed curves present the inelastic DM contributions with the DM mass-splitting $\Delta m = (2.5, 2.8, 3.0)$ keV, while the (green, red, blue) solid curves further include the XENON1T background contribution (shown as the black solid curve). The data points with error bars show the XENON1T measurement [2]. Plot (b): Constraints on our model by the direct DM detections of XENON1T, CRESST-III, CDEX-1B and DarkSide. The pink area shows the allowed region (95% C.L.) and the red solid curve gives the central value from fitting the XENON1T electron recoil data [2]. The gray regions are excluded at 90% C.L. by the nucleus recoil detections (of low threshold), where the (purple, light-blue, green, dark-blue) curves present the exclusion limits from the XENON1T [13], CRESST-III [16], CDEX-1B [15], and DarkSide-50 [14] experiments via nucleon recoils, respectively.

where e_R carries $U(1)_X$ charge $q_e = -\frac{1}{2}$. The $U(1)_X$ charge of the scalar DM is $q_{\text{DM}} = q_{\hat{\chi}} = 3$, and the fermionic DM has $q_{\text{DM}} = q_{\hat{\chi}} = \frac{3}{2}$. In Ref. [8], we used the effective field theory (EFT) approach to perform a model-independent fit of the inelastic DM for the XENON1T electron recoil spectrum [2]. Our fit shows that the XENON1T anomaly [2] can be fully explained by the two-component inelastic DM with mass-splitting $\Delta m \equiv m_{X'} - m_X = 2.8_{-0.3}^{+0.2}$ keV (68% C.L.) and $2.1 \text{ keV} < \Delta m < 3.3 \text{ keV}$ (95% C.L.). We obtain the ratio of the inelastic cross section over the DM mass, $\bar{\sigma}_e/m_X = (8.8 \pm 4.0) \times 10^{-44} \text{ cm}^2/\text{GeV}$, under the condition that the DM density contains equal amount of X and X' particles. Thus, by fitting the XENON1T data [2], we derive the following constraint on the current model:

$$\frac{m_{A'}}{g_X} = 1.2_{-0.1}^{+0.2} \times 10^2 \text{ GeV} \times \left[\left| \frac{q_e q_{\text{DM}}}{3/2} \right|^{\frac{1}{2}} \left(\frac{1 \text{ GeV}}{m_X} \right)^{\frac{1}{4}} \right]. \quad (13)$$

In Fig. 1(a), we present the electron recoil energy spectrum as predicted by the inelastic DM, in comparison with that of the XENON1T measurement [2]. The recoil spectra plotted in the (green, red, blue) dashed curves correspond to the inelastic DM contributions with the DM mass-splitting $\Delta m = (2.5, 2.8, 3.0)$ keV, whereas the (green, red, blue) solid curves further include the XENON1T background contribution (which is the black solid curve). The data points with error bars show the XENON1T measurement [2]. We have input a sample cross-section/mass ratio $\bar{\sigma}_e/m_X = 8.8 \times 10^{-44} \text{ cm}^2/\text{GeV}$,

which is the best fit with XENON1T data [2] as mentioned above Eq.(13). We note that the shape of our fitted recoil peak is mainly determined by the data points below 5 keV and the fit with the spectrum above 5 keV has little effect on the shape of this peak.

In Fig. 1(b), we show $m_{A'}/(g_X \sqrt{q_{\text{DM}}})$ as a function of the DM mass m_X . By fitting the recent XENON1T data [2], we present the allowed parameter space by the pink area at 95% C.L., and plot the central values (best fit) by the red solid curve. PandaX-II collaboration has accumulated 100.7 ton-day data from measuring the electron recoil spectrum [3] which is consistent with the background fluctuations. In each bin of the PandaX-II data, we find the expected DM signal rate to be less than 10 events/keV, which is smaller than the error bar. Hence, the best fit of our model is consistent with PandaX-II although its current bound is too weak to be shown in the same Fig. 1.

The DM particles in our model can also scatter with nuclei by exchanging the mediator A'_μ since the quarks (u_R, d_R) carry $U(1)_X$ charges as in Table I. The DM-nucleon scattering is dominated by the spin-independent interaction due to the mediator couplings with the DM and quarks. To compare with the nuclear recoil detection measurements, we compute the DM-nucleon scattering cross section as follows [17, 18],

$$\sigma_{\text{NX}} = \frac{m_N^2 m_X^2 q_{\text{DM}}^2 g_X^4}{16\pi (m_X + m_N)^2 m_{A'}^4}, \quad (14)$$

where $m_N \simeq 940 \text{ MeV}$ is the mass of nucleons.

For liquid scintillator experiments such as XENON1T [10] and DarkSide-50 [11], the nuclear recoil causes primary scintillation signals and are measured with energy thresholds at several keV, which are sensitive to DM particles with masses $\gtrsim 5$ GeV. Due to Migdal effect [12], the recoiled nuclei produce ionization and/or excitation of their atomic electrons with finite probability. The secondary radiation signals created by these electrons can be detected with much lower energy thresholds ($\lesssim 1$ keV), and thus largely enhance the sensitivity to sub-GeV DM. The strongest constraint is set by the recent XENON1T detection [13], which probes the light DM with masses down to about 85 MeV by measuring electronic recoils induced by the Migdal effect and bremsstrahlung. It can detect both scintillation and ionization signals as well as ionization signals only which allows for a lower detection threshold. The recent DarkSide-50 measurement [14] used a target of low-radioactivity argon and analyzed the ionization signals, which probes the light DM mass down to (1.8–6) GeV range. The CDEX-1B experiment [15] uses P -type point contact germanium (PPCGe) detectors to detect both the nuclear recoil energy and electron ionization energy. It can probe the light DM mass down to 50 MeV. Utilizing solid-state detectors with low energy thresholds is another significant means for light DM detection. The CRESST-III detection [16] operates scintillating CaWO_4 crystals as cryogenic calorimeters and can achieve a low nuclear recoil threshold energy of 30.1 eV. It is sensitive to the light DM of mass below ~ 2 GeV. In Fig. 1(b), we present the bounds (90% C.L.) from XENON1T [13], CRESST-III [16], CDEX-1B [15], and DarkSide-50 [14] on the parameter space of our model, shown by the gray region, over the mass range $m_X = (0.01 - 5)$ GeV. Here the purple, light-blue, yellow, and dark-blue curves give the 90% exclusion limits set by the XENON1T, CRESST-III, CDEX-1B, and DarkSide-50 experiments, respectively. We find that the XENON1T measurement imposes the strongest limit on our model.¹ This constrains the inelastic DM mass within the range $m_X \lesssim 1$ GeV.

IV. Analyzing Cosmological Constraints

In this section, we analyze the relevant cosmological constraints on the present inelastic DM model.

Lifetime of the Heavier DM Component X'

To resolve the XENON1T anomaly by inelastic DM, it is important to ensure that the lifetime of the heavier DM component X' is longer than the age of the Universe. Since we have the DM mass-splitting $\Delta m \ll m_e$,

only the decays such as $X' \rightarrow X\gamma\gamma$ and $X' \rightarrow X\nu\bar{\nu}$ are kinematically allowed. The decay channel $X' \rightarrow X\gamma\gamma$ occurs through one-loop diagrams with electron e_R or quarks u_R (d_R) running in the loop. Thus, with [8, 19], we can estimate the decay width of X' as

$$\Gamma_{X' \rightarrow X\gamma\gamma} \simeq \sum_{f=e,u,d} \frac{\eta_\gamma \alpha^2 g_X^4 q_{\text{DM}}^2}{15120\pi^5} \left(\frac{q_f N_{cf}}{m_f^2} \right)^2 \frac{\Delta m^9}{m_{A'}^4}, \quad (15)$$

where the sum runs over the electron-loop ($f = e$) and quark-loops ($f = u, d$), q_f denotes the electric charge of each fermion f , and the color factor $N_{cf} = 1$ (3) for the electron (quark) loop. The coefficient $\eta_\gamma = 1$ (1/36) for scalar (fermionic) DM. Since the quark masses $m_{u,d} \approx (1.5 - 6)$ MeV are much larger than the electron mass with the mass ratio $(m_e/m_{u,d})^4 = O(10^{-2} - 10^{-4})$, we see that the electron loop dominates the partial decay width (15). From fitting the XENON1T event rate, we have a small DM mass-splitting $\Delta m \simeq 3$ keV and the ratio of $m_{A'}/g_X$ given by Eq.(13). This leads to a tiny decay rate $\Gamma_{X' \rightarrow X\gamma\gamma} \approx (3\eta_\gamma \times 10^{23} \text{yr})^{-1}$, and thus $\Gamma_{X' \rightarrow X\gamma\gamma}^{-1} \gg \tau_U$, where $\tau_U \simeq 1.38 \times 10^{10} \text{yr}$ is the age of the Universe.

The other decay channel $X' \rightarrow X\nu\bar{\nu}$ occurs through the A' exchange due to the neutral gauge boson mixing matrix (5). The contribution of the Z exchange as induced by the mixing matrix (5) is fully negligible because of the large suppression factor $(m_{A'}^4/M_Z^4) \lesssim O(10^{-4})$ relative to the A' exchange. Thus, we can estimate the X' decay width as follows:

$$\Gamma_{X' \rightarrow X\nu\bar{\nu}} \simeq \frac{\eta_\nu q_{\text{DM}}^2 g_X^4}{160\pi^3} \frac{v_1^4 \Delta m^5}{v_h^4 m_{A'}^4}, \quad (16)$$

where we have included the contributions of the final state neutrinos from three families, and the factor $\eta_\nu = 1$ (2) for scalar (fermionic) DM. By requiring the X' lifetime be much longer than the age of our present universe, $\Gamma_{X' \rightarrow X\nu\bar{\nu}}^{-1} \gtrsim 10\tau_U \gg \tau_U$, we derive a constraint for the case of the scalar [fermionic] DM:

$$v_1 \lesssim 17 [15] \text{ GeV} \times \left(\frac{1 \text{ GeV}}{m_X} \right)^{\frac{1}{4}}. \quad (17)$$

This shows that in our model the electroweak symmetry breaking (EWSB) is mainly generated by the Higgs doublet H_2 , and the VEV ratio $\tan \beta = v_2/v_1 \gtrsim 10$.

Dark Matter Relic Abundance

Since our construction always holds $\Delta m \ll m_X$, the two DM components can be regarded as a degenerate complex scalar or Dirac spinor before they freeze out. We thus determine the relic density of a complex scalar \hat{X} or a Dirac spinor $\hat{\chi}$. We compute the DM relic density of the current model with the code `MicrOMEGAs` [17, 20] and present our results for the scalar DM model in Fig. 2. In plot (a), the blue curves show the masses of X (X') and A' which achieve the observed

¹ Note that for DM mass $\lesssim 1$ GeV, the typical recoil energy of scattering off an nucleus is below keV. We thus only include the down scattering process $X' + N \rightarrow X + N$ for the bound.

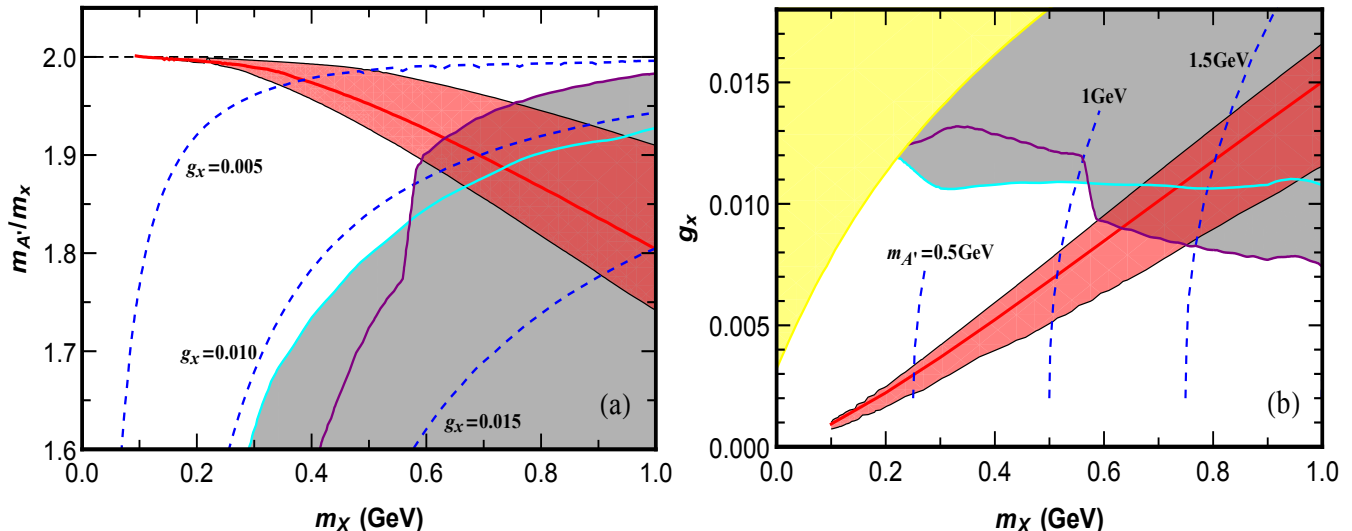


FIG. 2: Allowed parameter space for the inelastic scalar DM. In each plot, the pink areas depict the allowed regions (95% C.L.) by the XENON1T electron recoil data [2] combined with the DM relic density bound, and the red solid curve gives the best-fit values. The gray areas are excluded by nucleon recoil detections of low threshold (90% C.L.), where the purple and light blue curves are exclusion limits by XENON1T [13] and CRESST-III [16], respectively. Plot (a): Constraints on the parameter space of m_X versus $m_{A'}/m_X$. The blue dashed curves show the allowed parameter space of realizing the observed DM relic density for a set of sample g_X values. Plot (b): Constraints on the parameter space of m_X versus g_X . The blue dashed curves show the parameter space of realizing the observed DM relic density for a set of sample mediator masses $m_{A'}$. The yellow region is excluded by the DM relic density bound for $m_{A'}/m_X < 2$.

DM relic abundance, for each given value of the gauge coupling g_X . The pink area presents the allowed regions (95% C.L.) by the XENON1T data [2] combined with the DM relic density bound, and the red solid curve denotes the best-fit values. The gray region is excluded by the XENON1T [13] and CRESST-III [16] constraints under the condition of realizing the observed DM relic density by proper choice of g_X . We find that the DM mass range $m_X \lesssim 0.75$ GeV is favored in our model, and in the viable parameter space the dominant DM annihilation channel is $\hat{X}^* \hat{X} \rightarrow A' \rightarrow f_R \bar{f}_R$, where $f = u, d, e$. In plot (b), the pink region presents the allowed parameter space of m_X versus g_X at 95% C.L., and the red solid curve gives the best-fit values. The blue curves show the allowed values of the gauge coupling g_X as a function of the DM mass m_X , which achieve the observed DM relic abundance for each given mediator mass $m_{A'}$. We fit the XENON1T electron recoil data [2] and DM relic density bound together, and include the constraints of $m_X \lesssim 0.75$ GeV by XENON1T [13] and CRESST-III [16] nuclear recoil measurements (the gray area). With these, we derive the combined limit $g_X \lesssim 0.013$ for the case $m_{A'}/m_X > 2$, and $g_X \lesssim 0.009$ for the case $m_{A'}/m_X < 2$.

In Fig. 3, we present our results for the inelastic fermionic DM. Similar to the scalar DM case, the annihilation of fermionic DM in the viable parameter space is dominated by the s -channel process $\hat{\chi}^\dagger \hat{\chi} \rightarrow A' \rightarrow f_R \bar{f}_R$. But, the annihilation is more efficient in the case of fermionic DM because it is s -wave dominant; whereas for the scalar DM, the process is p -wave dominant due to

its derivative coupling. In order to achieve the observed DM relic density, the parameters for the fermionic DM have to be farther away from the resonance than that for the scalar DM. Hence, in Fig. 3(a) the viable parameter region (pink area) for the fermionic DM covers lower values of the mass ratio $m_{A'}/m_X$, as compared to that in Fig. 2(a).

Current Ratio of X and X'

Next, we examine whether the constrained couplings in Figs. 2-3 are consistent with the condition $n_X = n_{X'}$. After the decoupling of the annihilation process $\hat{X} \hat{X}^\dagger \rightarrow f_R \bar{f}_R$, the total DM number density $n_{\hat{X}} = n_X + n_{X'}$ is fixed. But, X and X' can still convert to each other through the processes $e^\pm X \leftrightarrow e^\pm X'$ and $X' X' \leftrightarrow X X$. As we showed previously [8], the former process decouples at $T \sim m_e$ ($\gg \Delta m$) for the GeV scale DM. The latter process is induced by t - and u -channel exchanges of A' . If the annihilation $X' X' \rightarrow X X$ decouples at a temperature $T' < \Delta m$, the X' density would be exponentially suppressed by a factor of $\exp(-\Delta m/T')$. As an estimate, this process becomes inefficient when the reaction rate $\Gamma(T') \lesssim H(T')$. We estimate this reaction rate as $\Gamma(T') \simeq \langle \sigma' v_{\text{DM}} \rangle n_{\text{DM}}$, in which the thermally averaged DM annihilation cross section $\langle \sigma' v_{\text{DM}} \rangle \simeq g_X^4 q_{\text{DM}}^4 \sqrt{m_X^3 T'} / (\pi m_{A'}^4)$ and the DM density $n_{\text{DM}} \simeq T_{\text{eq}}^3 / m_X$. Here T_{eq} is the temperature at the matter-radiation equality. Thus, with these and Eq. (13), we can estimate

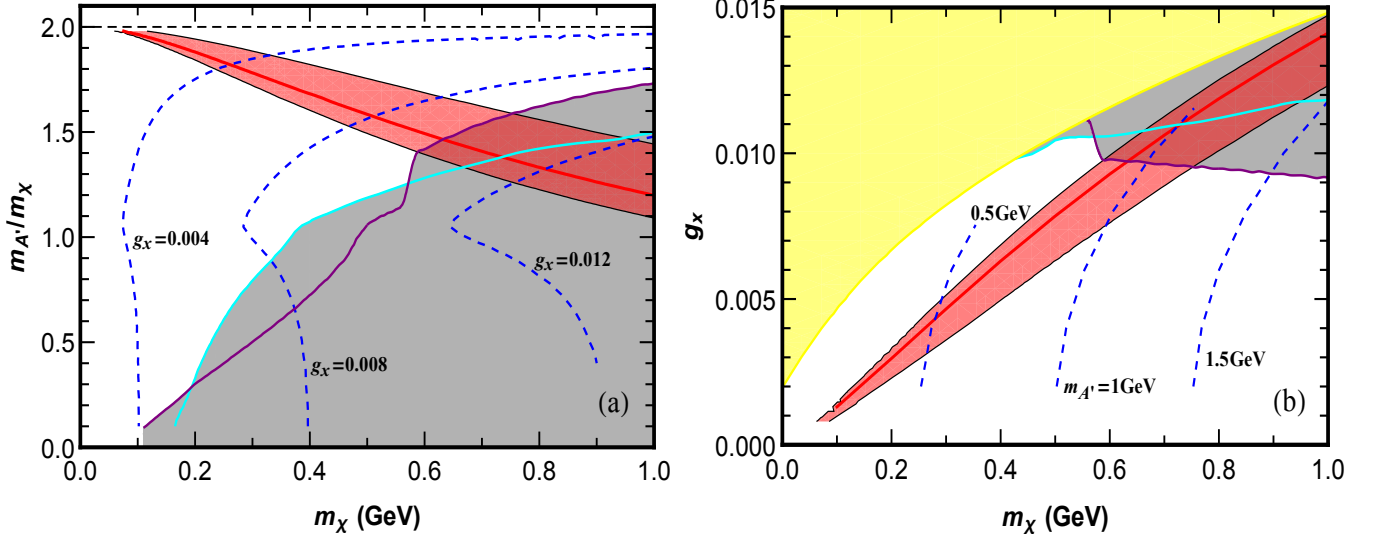


FIG. 3: Allowed viable parameter space for the inelastic fermionic DM, as shown in plots (a) for m_X versus $m_{A'}/m_X$, and in plots (b) for m_X versus g_X . The curves and shaded regions have the same meanings as defined in the caption of Fig. 2 except the current plots present the case of the inelastic fermionic DM.

$$T' \approx 0.01 \text{ GeV} \times \left(\frac{1 \text{ GeV}}{m_X} \right) \times \left(\frac{3}{q_{\text{DM}}} \right)^{\frac{4}{3}}. \quad (18)$$

Shortly after the kinetic decoupling, the DM temperature drops rapidly as $a(t)^{-2}$ and falls below Δm quickly. The X' density would get depleted if the annihilation $X'X' \rightarrow XX$ is still efficient. As a conservative estimate, we demand $T' \gtrsim m_e$, so the process $X'X' \rightarrow XX$ decouples before the kinetic decoupling between e^\pm and the DM. This imposes an upper bound $m_X \lesssim 20$ (50) GeV for scalar (fermionic) DM, which is always satisfied in our model.

V. Analyzing Laboratory Constraints

In this section, we proceed to analyze the relevant laboratory constraints on our inelastic DM models.

Correction to Z Boson Mass

Our model contributes to several electroweak precision observables. Using Eq.(4), we derive the new correction to Z boson mass:

$$\delta M_Z = \frac{g_X^2 v_1^4}{4v_h^2 M_Z}. \quad (19)$$

The Z pole observables have been measured with high precision. Especially, the SM fit with the precision data gives the prediction $M_Z^{\text{sm}} = (91.1884 \pm 0.0020)$ GeV, while the direct measurement of Z boson mass gives $M_Z^{\text{exp}} = (91.1876 \pm 0.0021)$ GeV [21]. This strongly constrains any new physics contribution to Z mass, $\delta M_Z < 0.0049$ GeV at 95% C.L. Thus, we derive an upper bound on the VEV of the Higgs doublet H_1 ,

$$v_1 \lesssim 15.2 \text{ GeV} / \sqrt{g_X}. \quad (20)$$

Correction to Electron Anomalous Magnetic Moment

The $U(1)_X$ interaction also alters the anomalous magnetic moments of electrons. For $m_{A'} \gg m_e$, we can derive the one-loop correction to $a_e = \frac{1}{2}(g_e - 2)$:

$$\delta a_e^X \simeq -\frac{g_X^2 q_e^2}{12\pi^2} \frac{m_e^2}{m_{A'}^2}, \quad (21)$$

with $q_e = -\frac{1}{2}$, which agrees with [22]. For $(g_X, m_{A'})$ obeying Eq.(13) and for the scalar (fermionic) DM having $U(1)_X$ charge $q_{\text{DM}}=3$ (3/2), we derive the correction to the electron anomalous magnetic moment,

$$\delta a_e^X \simeq 3.8 (7.6) \times 10^{-14} \times \sqrt{m_X / (1 \text{ GeV})}, \quad (22)$$

which is lower than the current experimental sensitivity of 10^{-13} [21].

Other Constraints on the Higgs Sector

There are additional bounds that can constrain the Higgs sector of our inelastic DM model. For instance, the signal strength of the SM-like Higgs boson $h(125\text{GeV})$ measured at the LHC can constrain the mixing between the CP-even neutral component of H_2 and the other scalar singlets. The flavor-dependent feature of our two-Higgs-doublet sector could induce the flavor-changing processes via Higgs-exchange, so the mass of the heavy neutral Higgs (mainly from H_1 doublet) is constrained by meson mixings. Since the present study focuses on analyzing the DM and its vector portal to the SM particles, we note that these constraints can be satisfied by proper parameter choice in the Higgs sector, which will

be elaborated in Appendix A.

Collider Constraints

Since the mediator A'_μ couples directly to the right-handed electrons, our model will receive nontrivial tests by the e^+e^- collider measurements. (There are discussions on constraining light DM models at lepton colliders in the literature [23–25].) The mediator A'_μ contributes constructively to the cross section of $e^+e^- \rightarrow e^+e^-$. This cross section has been measured by LEP [26], with which we infer a bound on our model, $\sqrt{4\pi s}/(|q_e|g_X) > 8.6$ TeV at 95% C.L.,² where $\sqrt{s} \simeq 200$ GeV is the LEP collider energy, and $q_e = -\frac{1}{2}$ is the $U(1)_X$ charge of e_R in our model. From this we deduce an upper bound on the $U(1)_X$ gauge coupling, $g_X \lesssim 0.16$.

The DM particles can be pair-produced in e^+e^- collisions through s -channel $A'(Z)$ -exchanges and in association with the final state mono-photon, $e^+e^- \rightarrow XX'\gamma$. The rate of the DM production with mono-photon via Z -exchange is highly suppressed by a coupling factor v_1^4/v_h^4 which arises from the gauge boson mixing matrix (5). As we have shown in Sec. IV and Fig. 2-3, the A' mass has to be less than a few GeV due to the combined bounds of realizing the DM relic density and fitting the DM direct detection data. We find that for the contribution of A' exchange in the case of $\sqrt{s} > m_{A'} > 2m_X$ at LEP [27], the cross section of this process has a resonance at $E_\gamma/E_{\text{beam}} \sim 1 - m_{A'}^2/s$. By fitting the LEP mono-photon data with parameters obeying the relic density bound, we derive the 95% exclusion limit on our models, $g_X \lesssim 0.015$. On the other hand, we find that in the parameter region $m_{A'} < 2m_X$ and under the DM relic density bound, the contribution to the LEP mono-photon process is too small to receive constraint, so this region is always allowed. The mono-photon searches at low energy e^+e^- colliders such as BaBar [28] and Belle-II [29] can also place nontrivial bounds on models of light DM [24]. We summarize these bounds on our model as follows, according to Ref. [24]. For the mass region $m_X \lesssim 1$ GeV and $m_{A'} \lesssim 2m_X$, the BaBar measurements constrain $g_X^2|q_e|q_{\text{DM}} < O(10^{-2})$. For the on-going Belle-II experiment, the projected constraint set by null result is $g_X^2q_eq_{\text{DM}} < O(10^{-3})$, assuming that the backgrounds are ideally known. As shown in Sec. IV, for this case, combining the constraints from the DM direct detections and realizing the DM relic density will require $g_X \lesssim 0.01$, which satisfies all the e^+e^- collider bounds. For the mass range $m_{A'} > 2m_X$, the BaBar experiment sets strong constraint on the $A' - e^\pm$ coupling. It is stronger than LEP mono-photon search limit, due to the much larger production cross section and the much higher integrated luminosity of BaBar. Given our charge assignment $q_e = 1/2$ and the

branching fraction of $A' \rightarrow XX'$, we can derive the corresponding constraint on our model, $g_X \lesssim 0.003$. Combined with the bounds from the XENON1T electron recoil and DM relic density, the BaBar bound on g_X further constrains the DM and mediator masses $m_X < 0.25$ GeV and $m_{A'} < 0.68$ GeV for the inelastic scalar DM, and $m_X < 0.21$ GeV and $m_{A'} < 0.55$ GeV for the inelastic fermionic DM. Thus, the $m_{A'} > 2m_X$ region is mostly excluded.

The LHC measurement of $Z \rightarrow 4\mu$ decays [30] can constrain the coupling between A'_μ and μ^\pm . This coupling is induced from the neutral gauge boson mixing matrix (5) and the corresponding Lagrangian term is

$$\mathcal{L} \supset \frac{g_X v_1^2}{v_h^2} \bar{\mu} \gamma^\mu \left[(\sin^2 \theta_W - \frac{1}{4}) + \frac{1}{4} \gamma^5 \right] A'_\mu \mu. \quad (23)$$

For a vector-type new interaction $g_{\text{new}} \bar{\mu} \gamma^\mu A'_\mu \mu$ and the small mediator mass $m_{A'} < 10$ GeV, the LHC has placed a bound on its coupling, $g_{\text{new}} \lesssim 4.5 \times 10^{-3}$ at 95% C.L. For $v_1^2/v_h^2 = 10^{-2}$, we convert this LHC bound to a constraint on the $U(1)_X$ coupling of our model, $g_X \lesssim O(1)$, which is weaker than the combined bound via direct detections and relic density. The inelastic DM particles of our model can also be directly produced at the LHC through its coupling to the right-handed quarks (u_R, d_R), giving raise to mono-photon signals together with the missing P_T . Such signals have been actively searched by ATLAS [31] and CMS [32]. But, these searches lose sensitivity for $g_X < O(0.1)$ [33] and does not constrain the cosmologically favored parameter space as discussed in Sec. IV.

VI. Conclusions

In this work, we proposed a new candidate of GeV scale inelastic dark matter (DM), which can be either scalars or fermions. For this we constructed anomaly-free and renormalizable inelastic DM models under an extra $U(1)_X$ gauge symmetry with a dark photon mediator and for scalar or fermionic DM particles (cf. Table I). We realized the natural $O(\text{keV})$ mass-splitting for the inelastic DM by a scalar seesaw mechanism without fine-tuning. Our model resolved the recent XENON1T anomaly [2] via electron recoil detection. It is highly testable and we further analyzed the nontrivial bounds from the nuclear recoil detection by the XENON1T [13], CRESST-III [16], CDEX-1B [15], and DarkSide-50 [14] experiments with low recoil energy thresholds. Combining the constraints from both the electron recoil and nuclear recoil detections, we identified the viable parameter space and predicted the inelastic DM mass $\lesssim 1$ GeV, as shown in Fig. 1. Then, we derived the viable parameter space in Fig. 2 for the scalar inelastic DM and Fig. 3 for the fermionic inelastic DM, under the constraints by the DM relic abundance, the lifetime of the heavier DM component, the electroweak precision tests, and the collider searches. The upcoming DM direct detection measurements by the

² Hereafter all the quoted experimental bounds are set at 95% C.L. unless specified otherwise.

PandaX-4T [34], LZ [35], and XENONnT [36] collaborations will provide decisive probes of our GeV scale inelastic DM candidate.

Acknowledgements

We thank Jianglai Liu, Qian Yue, and Ning Zhou for useful discussions on DM direct detections. This research was supported in part by National NSF of China (under grants Nos. 11835005 and 11675086), by National Key R&D Program of China (under grant No. 2017YFA0402204), and by the CAS Center for Excellence in Particle Physics (CCEPP). It was also supported in part by Office of Science and Technology, Shanghai Municipal Government (No. 16DZ2260200).

A. Constraints on the Higgs Sector

In this Appendix, we present the constraints on the Higgs sector of our model. For convenience, we denote the CP-even neutral components of (H_1, H_2, S') as $(h_1, h_2, h_{S'})$, respectively. We consider the case of $M_{h_1}^2 \gg M_{h_2}^2$ and $v_1^2 \ll v_2^2$, so the observed Higgs boson $h(125\text{GeV})$ mainly contains the h_2 state. To realize these conditions, we consider the relevant part of the scalar potential,

$$V \supset M_{H_1}^2 |H_1|^2 - M_{H_2}^2 |H_2|^2 - M_{S'}^2 |S'|^2 - M' H_1^\dagger H_2 S' \\ + \lambda_1 |H_1|^4 + \lambda_2 |H_2|^4 + \lambda_3 |H_1|^2 |H_2|^2 + \lambda_{S'} |S'|^4 \\ + \lambda_{H_1 S'} |H_1|^2 |S'|^2 + \lambda_{H_2 S'} |H_2|^2 |S'|^2, \quad (\text{A1})$$

where we only list terms relevant to H_1, H_2 and S' . The cubic term $H_1^\dagger H_2 S'$ will ensure nonzero mass of the pseudoscalars. In Eq.(A1), we take all the mass parameters and the quartic couplings be positive. We choose the Higgs doublet H_1 to have a large positive mass term with $M_{H_1}^2 \gg v_2^2, v_{S'}^2$. Thus, we deduce the VEV of H_1 ,

$$v_1 \simeq \frac{v_2 v_{S'} M'}{M_{H_1}^2}. \quad (\text{A2})$$

We see that requiring $M_{H_1}^2 \gg M' v_{S'}$, can realize $v_1^2 \ll v_2^2$. ATLAS and CMS have measured the signal strength of the Higgs boson $h(125\text{GeV})$ for various channels, defined as $\mu_h \equiv \langle \sigma_h \cdot \text{BR} \rangle_{\text{obs}} / \langle \sigma_h \cdot \text{BR} \rangle_{\text{SM}}$, with σ_h the h production cross section and BR the decay branching fraction of a given channel. The most precisely measured channels are $\gamma\gamma$ and WW^* which are consistent with the SM ($\mu_h=1$) to 10% level [21]. This constrains the mixings of the SM-like Higgs boson h_2 with $h_{S'}$ and h_1 down to 10% level. Note that for $v_1^2 \ll v_2^2$, the h_2 - h_1 mixing is mainly generated by the cubic term $-M' H_1^\dagger H_2 S'$, and the contributions from the mixed quartic terms are suppressed by v_1/M' . Thus, for $M_{H_1}^2 \gg M_{H_2}^2$, the h_2 - h_1 mixing is mainly determined by $|M' v_{S'} / M_{H_1}^2| \simeq v_1 / v_2$. With this condition, we may choose the VEV ratio

$$v_1 / v_2 \lesssim 0.1. \quad (\text{A3})$$

The small h_2 - $h_{S'}$ mixing can be induced by the contributions from the cubic and quartic terms with opposite signs. As an estimate, we ignore the small mixing of the heavy h_1 with the lighter states h_2 or $h_{S'}$ and obtain,

$$|\sin \theta_{h_2 h_{S'}}| \simeq \left| \frac{\lambda_{H_2 S'} v_2 v_{S'} - M' v_1}{M_h^2 - M_{h_{S'}}^2} \right| \ll 1. \quad (\text{A4})$$

Another constraint on the heavy Higgs mass M_{H_1} comes from the flavor-changing processes mediated by the heavy scalars. The general Yukawa interactions for the quark sector take the following form,

$$\mathcal{L} = - \sum_{i=1}^3 \left(y_u^{i1} \bar{Q}_{Li} \tilde{H}_1 u_{R1} + y_d^{i1} \bar{Q}_{Li} H_1 d_{R1} \right) \\ - \sum_{i=1,2,3}^{j=2,3} \left(y_u^{ij} \bar{Q}_{Li} \tilde{H}_2 u_{Rj} + y_d^{ij} \bar{Q}_{Li} H_2 d_{Rj} \right) \quad (\text{A5a})$$

$$\equiv - \bar{Q}_L^i \left(\tilde{\mathbf{y}}_u \tilde{H}_1, \hat{\mathbf{y}}_u \tilde{H}_2 \right)_{ij} u_{Rj} - \bar{Q}_L^i \left(\tilde{\mathbf{y}}_d H_1, \hat{\mathbf{y}}_d H_2 \right)_{ij} d_{Rj} \quad (\text{A5b})$$

where we denote $\tilde{H}_i = i\sigma_2 H_i^*$. For convenience, in the last line, we have decomposed the 3×3 Yukawa matrix $\mathbf{y}^{\mathbf{u},\mathbf{d}} = (\tilde{\mathbf{y}}_{\mathbf{u},\mathbf{d}}, \hat{\mathbf{y}}_{\mathbf{u},\mathbf{d}})_{ij}$. Here, $\tilde{\mathbf{y}}_{\mathbf{u},\mathbf{d}}$ are 3×1 matrices of Yukawa couplings to H_1 and $\hat{\mathbf{y}}_{\mathbf{u},\mathbf{d}}$ are 3×2 matrices of Yukawa couplings to H_2 . The quarks acquire masses via Yukawa interactions with H_1 and H_2 taking their VEVs. The mass eigenstates are obtained by chiral rotations,

$$\mathbf{u}'_L = U_L^u \mathbf{u}_L, \quad \mathbf{d}'_L = U_L^d \mathbf{d}_L, \quad (\text{A6a})$$

$$\mathbf{u}'_R = U_R^{u\dagger} \mathbf{u}_R, \quad \mathbf{d}'_R = U_R^{d\dagger} \mathbf{d}_R, \quad (\text{A6b})$$

where \mathbf{u} and \mathbf{d} are vectors in flavor space denoting the 3 family of quarks, and $U_{L,R}^{u,d}$ are unitary rotation matrices. The quark mass matrices are diagonalized as

$$U_L^{u\dagger} \left(\tilde{\mathbf{y}}_u v_1, \hat{\mathbf{y}}_u v_2 \right) U_R^u = v_2 \mathbf{y}_u^{\text{diag}}, \quad (\text{A7a})$$

$$U_L^{d\dagger} \left(\tilde{\mathbf{y}}_d v_1, \hat{\mathbf{y}}_d v_2 \right) U_R^d = v_2 \mathbf{y}_d^{\text{diag}}, \quad (\text{A7b})$$

where $v_2 \mathbf{y}_{\mathbf{u}(\mathbf{d})}^{\text{diag}}$ is the 3×3 diagonal mass matrix for up-type (down-type) quarks, whose diagonal elements give the measured quark masses. In the mass-eigenbasis, the Yukawa interactions for the up-type quarks become:

$$\mathcal{L} = - \bar{\mathbf{u}}'_L U_L^{u\dagger} \left(\tilde{\mathbf{y}}_u \tilde{H}_1^0, \hat{\mathbf{y}}_u \tilde{H}_2^0 \right) U_R^u \mathbf{u}'_R \quad (\text{A8a})$$

$$= - \bar{\mathbf{u}}'_L U_L^{u\dagger} \left[\tilde{\mathbf{y}}_u \left(\tilde{H}_1^0 - \frac{v_1}{v_2} \tilde{H}_2^0 \right), (\mathbf{0}) \right] U_R^u \mathbf{u}'_R \\ - \bar{\mathbf{u}}'_L \mathbf{y}_u^{\text{diag}} \tilde{H}_2^0 \mathbf{u}'_R, \quad (\text{A8b})$$

where \tilde{H}_1^0 and \tilde{H}_2^0 denote the neutral components of the Higgs doublets \tilde{H}_1 and \tilde{H}_2 , respectively. Similarly, we can deduce the Yukawa interactions for the mass-eigenstates of down-type quarks under the replacement $\mathbf{u} \rightarrow \mathbf{d}$ and $\tilde{H}_i \rightarrow H_i$. In Eq.(A8b), $(\mathbf{0})$ denotes a 3×2

matrix in which all elements vanish. The first term in Eq.(A8b) would induce flavor-changing processes if the flavor mixing matrices $U_{L,R}^u$ take arbitrary pattern, and in this case it will receive strong constraints by the meson mixings. It is known that for well-motivated scenarios of flavor mixing such constraints can be much reduced. For instance, we may consider Cheng-Sher-like ansatz [37][38] on the flavor-changing Yukawa couplings,

$$\xi_{u,d}^{ij} = \bar{\xi}_{u,d}^{ij} \times \left(\sqrt{m_{u,d}^i m_{u,d}^j} / v_h \right), \quad (\text{A9})$$

where (i, j) are family indices and the coupling coefficients $\bar{\xi}_{u,d}^{ij}$ are naturally around $\bar{\xi}_{u,d}^{ij} = O(0.1-1)$ without fine-tuning. Thus, we set

$$U_L^{u,d\dagger} \left(\vec{y}_{u,d}, \mathbf{0} \right) U_R^{u,d} = \xi_{u,d}. \quad (\text{A10})$$

Then, the flavor-changing process between the i -th and j -th families is characterized by the new physics (NP) scale,

$$\Lambda_{\text{NP}} = \min \left(M_{h_1}, \frac{v_2}{v_1} M_{h_2} \right) \frac{\bar{\xi}_{u,d}^{ij} v_h}{\sqrt{m_{u,d}^i m_{u,d}^j}}, \quad (\text{A11})$$

where the $M_{h_1} = O(\text{TeV})$ is the mass of the heavy neutral Higgs state h_1 and $M_{h_2} \simeq 125 \text{ GeV}$ is the SM-like light Higgs boson h_2 . For instance, the measurements of $K-\bar{K}$ mixing constrain $\Lambda_{\text{NP}} \gtrsim 5 \times 10^5 \text{ TeV}$ [39]. With this bound and for a natural coupling coefficient $\bar{\xi}_d^{12} = O(0.1)$, we obtain the limits on our Higgs sector, $M_{h_1} \gtrsim 6 \text{ TeV}$ and $v_1 \lesssim 3.6 \text{ GeV}$. The $U(1)_X$ gauge boson A'_μ also mediates flavor-violating process since it only couples to the right-handed quarks and leptons in the first family. The ratio $m_{A'}/g_X$ is constrained by fitting the XENON1T data as in Eq.(13). So the constraints from the meson mixing measurements could be avoided by requiring the right-handed mass-eigenstates u'_R and d'_R to be mainly aligned with the gauge-eigenstates u_R and d_R . In addition, we note that the flavor-violating effects can also occur in the lepton sector and induces flavor-violating leptonic decay channels for the SM-like light Higgs boson h_2 . For instance, this leads to the interesting decay channel $h_2 \rightarrow \mu^\pm e^\mp$, which can be searched by analyzing the current LHC Run-2 data [40]. The upcoming LHC Run-3 and HL-LHC runs will have strong potential to discover this channel.

-
- [1] E. Aprile *et al.* [XENON Collaboration], “Energy resolution and linearity in the keV to MeV range measured in XENON1T”, *Eur. Phys. J. C* 80 (2020) 785, no.8 [arXiv:2003.03825 [physics.ins-det]].
- [2] E. Aprile *et al.* [XENON Collaboration], “Observation of Excess Electronic Recoil Events in XENON1T”, *Phys. Rev. D* 102 (2020) 072004, no.7, [arXiv:2006.09721 [hep-ex]].
- [3] X. Zhou *et al.* [PandaX-II Collaboration], “A search for solar axions and anomalous neutrino magnetic moment with the complete PandaX-II data”, arXiv:2008.06485 [hep-ex].
- [4] A. E. Robinson, arXiv:2006.13278 [hep-ex].
- [5] K. Kannike, M. Raidal, H. Veermae, A. Strumia, and D. Teresi, “Dark Matter and the XENON1T electron recoil excess”, *Phys. Rev. D* 102 (2020) 095002, no.9 [arXiv:2006.10735 [hep-ph]].
- [6] L. Di Luzio, M. Fedele, M. Giannotti, F. Mescia and E. Nardi, arXiv:2006.12487 [hep-ph]. F. Takahashi, M. Yamada and W. Yin, arXiv:2006.10035 [hep-ph]; G. Alonso-Alvarez, F. Ertas, J. Jaeckel, F. Kahlhoefer, and L. J. and Thormaehlen, arXiv:2006.11243 [hep-ph]; C. Boehm, D. G. Cerdeno, M. Fairbairn, P. A. N. Machado, and A. C. Vincent, arXiv:2006.11250 [hep-ph]; D. A. Sierra, V. De Romeri, L. J. Flores, and D. K. Papoulias, arXiv:2006.12457 [hep-ph]; B. Fornal, P. Sandick, J. Shu, M. Su, and Y. Zhao, arXiv:2006.11264 [hep-ph]; L. Su, W. Wang, L. Wu, J. M. Yang and B. Zhu, arXiv:2006.11837 [hep-ph]; Y. Chen, J. Shu, X. Xue, G. Yuan, and Q. Yuan, arXiv:2006.12447 [hep-ph]; Q. H. Cao, R. Ding, and Q. F. Xiang, arXiv:2006.12767 [hep-ph]; H. Alhazmi, D. Kim, K. Kong, G. Mohlabeng, J. C. Park and S. Shin, arXiv:2006.16252 [hep-ph]; Y. Jho, J. C. Park, S. C. Park, and P. Y. Tseng, arXiv:2006.13910 [hep-ph]; S. Chigusa, M. Endo and K. Kohri, arXiv:2007.01663 [hep-ph]. J. Smirnov and J. F. Beacom, arXiv:2002.04038 [hep-ph]; A. Bally, S. Jana, and A. Trautner, arXiv:2006.11919 [hep-ph]; M. Du, J. Liang, Z. Liu, V. Q. Tran, and Y. Xue, arXiv:2006.11949 [hep-ph]; D. Aristizabal Sierra, V. De Romeri, L. J. Flores, and D. K. Papoulias, arXiv:2006.12457 [hep-ph]; N. F. Bell, J. B. Dent, B. Dutta, S. Ghosh, J. Kumar, and J. L. Newstead, arXiv:2006.12461 [hep-ph]; G. Paz, A. A. Petrov, M. Tamaro, and J. Zupan, arXiv:2006.12462 [hep-ph]; J. Buch, M. A. Buen-Abad, J. Fan, and J. S. C. Leung, arXiv:2006.12488 [hep-ph]; K. U. Dey, T. N. Maity, and T. S. Ray, arXiv:2006.12529 [hep-ph]; A. N. Khan, arXiv:2006.12887 [hep-ph]; K. Nakayama and Y. Tang, arXiv:2006.13159 [hep-ph]; L. Zu, G. W. Yuan, L. Feng and Y. Z. Fan, arXiv:2006.14577 [hep-ph]; M. Lindner, Y. Mambrini, T. B. Melo, and F. S. Queiroz, arXiv:2006.14590 [hep-ph]. W. DeRocco, P. W. Graham, S. Rajendran, arXiv:2006.15112 [hep-ph]; M. Chala and A. Titov, arXiv:2006.14596 [hep-ph]; C. Gao, J. Liu, L. T. Wang, X. P. Wang, W. Xue, and Y. M. Zhong, arXiv:2006.14598 [hep-ph]; J. B. Dent, B. Dutta, J. L. Newstead, and A. Thompson, arXiv:2006.15118 [hep-ph]; P. Ko and Y. Tang, arXiv:2006.15822 [hep-ph]; W. Chao, Y. Gao, and M. Jin, arXiv:2006.16145 [hep-ph]; L. Delle Rose, G. Hütsi, C. Marzo, and L. Marzola, arXiv:2006.16078 [hep-ph]; B. Bhattacharjee and R. Sengupta, arXiv:2006.16172 [hep-ph]; Y. Gao and T. Li, arXiv:2006.16192 [hep-ph]; J. Sun and X. G. He, arXiv:2006.16931 [hep-ph]; M. Szydagis, C. Levy, G. M. Blockinger, A. Kamaha, N. Parveen, and G. R. C. Rischbieter, arXiv:

- 2007.00528 [hep-ex]; T. Li, arXiv:2007.00874 [hep-ph]; O. G. Miranda, D. K. Papoulias, M. Tortola, and J. W. F. Valle, arXiv:2007.01765 [hep-ph]; K. Benakli, C. Branchina and G. Lafforgue-Marmet, arXiv:2007.02655 [hep-ph]; N. Okada, S. Okada, D. Raut, and Q. Shafi, arXiv:2007.02898 [hep-ph]; J. Davighi, M. McCullough, and J. Tooby-Smith, arXiv:2007.03662 [hep-ph]; P. Athron, *et al.*, arXiv:2007.05517 [astro-ph.CO]; G. Arcadi, A. Bally, F. Goertz, K. Tame-Narvaez, V. Tenorth and S. Vogl, arXiv:2007.08500 [hep-ph]; C. Han, M. L. Lopez-Ibanez, A. Melis, O. Vives and J. M. Yang, arXiv:2007.08834 [hep-ph]; Y. Ema, F. Sala and R. Sato, arXiv:2007.09105 [hep-ph]; J. Kim, T. Nomura and H. Okada, arXiv:2007.09894 [hep-ph]; J. Cao, X. Du, Z. Li, F. Wang and Y. Zhang, arXiv:2007.09981 [hep-ph]; D. Borah, S. Mahapatra, D. Nanda and N. Sahu, arXiv:2007.10754 [hep-ph]. S. Karmakar and S. Pandey, arXiv:2007.11892 [hep-ph]; S. Khan, arXiv:2007.13008 [hep-ph]; S. Shakeri, F. Hajkarim, and S. S. Xue, arXiv:2008.05029 [hep-ph]; R. G. Cai, S. Sun, B. Zhang, and Y. L. Zhang, arXiv:2009.02315 [hep-ph]; R. Foot, arXiv:2011.02590 [hep-ph]. Y. Farzan and M. Rajae, arXiv:2007.14421 [hep-ph].
- [7] K. Harigaya, Y. Nakai and M. Suzuki, arXiv:2006.11938 [hep-ph]; H. M. Lee, arXiv: 2006.13183 [hep-ph]; M. Baryakhtar, A. Berlin, H. Liu and N. Weiner, arXiv:2006.13918 [hep-ph]; J. Bramante and N. Song, arXiv:2006.14089 [hep-ph]; I. M. Bloch, A. Caputo, R. Essig, D. Redigolo, M. Sholapurkar, and T. Volansky, arXiv:2006.14521 [hep-ph]; H. An and D. Yang, arXiv:2006. 15672 [hep-ph]; S. Baek, J. Kim, and P. Ko, arXiv:2006. 16876 [hep-ph]; A. Aboubrahim, M. Klasen and P. Nath, arXiv:2011.08053 [hep-ph].
- [8] H. J. He, Y. C. Wang, and J. Zheng, JCAP (2021), in press, [arXiv:2007.04963].
- [9] T. Gherghetta, J. Kersten, K. Olive, and M. Pospelov, Phys. Rev. D 100 (2019) 095001, no.9 [arXiv:1909.00696 [hep-ph]].
- [10] E. Aprile *et al.* [XENON Collaboration], Phys. Rev. Lett. 121 (2018) 111302 [arXiv:1805.12562 [astro-ph.CO]].
- [11] P. Agnes *et al.* [DarkSide Collaboration], Phys. Rev. D 93 (2016) 081101, no.8 [arXiv:1510.00702 [astro-ph.CO]].
- [12] A. B. Migdal, J. Phys. (USSR) 4 (1941) 449; M. Ibe, W. Nakano, Y. Shoji, and K. Suzuki, JHEP 03 (2018) 194 [arXiv:1707.07258 [hep-ph]]; M. J. Dolan, F. Kahlhoefer, C. McCabe, Phys. Rev. Lett. 121 (2018) 101801, [arXiv:1711.09906 [hep-ph]].
- [13] E. Aprile *et al.* [XENON Collaboration], Phys. Rev. Lett. 123 (2019) 241803, no.24 [arXiv:1907.12771 [hep-ex]].
- [14] P. Agnes *et al.* [DarkSide Collaboration], Phys. Rev. Lett. 121 (2018) 081307, no.8 [arXiv:1802.06994 [astro-ph.HE]].
- [15] Z. Z. Liu *et al.* [CDEX Collaboration], Phys. Rev. Lett. 123 (2019) 161301, no.16 [arXiv:1905.00354 [hep-ex]].
- [16] A. H. Abdelhameed *et al.* [CRESST Collaboration], Phys. Rev. D 100 (2019) 102002, no.10 [arXiv:1904.00498 [astro-ph.CO]].
- [17] G. Belanger, F. Boudjema, A. Pukhov, and A. Semenov, Comput. Phys. Commun. 180 (2009) 747 [arXiv:0803.2360 [hep-ph]].
- [18] Z. H. Yu, J. M. Zheng, X. J. Bi, Z. Li, D. X. Yao, and H. H. Zhang, Nucl. Phys. B 860 (2012) 115 [arXiv:1112.6052 [hep-ph]].
- [19] C. B. Jackson, G. Servant, G. Shaughnessy, T. Tait, and M. Taoso, JCAP 07 (2013) 021 [arXiv:1302.1802].
- [20] G. Belanger, A. Mjallal and A. Pukhov, arXiv:2003.08621 [hep-ph].
- [21] M. Tanabashi *et al.* [Particle Data Group], Phys. Rev. D 98 (2018) 030001.
- [22] J. P. Leveille, Nucl. Phys. B 137 (1978) 63.
- [23] P. J. Fox, R. Harnik, J. Kopp and Y. Tsai, “LEP Shines Light on Dark Matter,” Phys. Rev. D 84 (2011) 014028 [arXiv:1103.0240 [hep-ph]].
- [24] R. Essig, J. Mardon, M. Papucci, T. Volansky, and Y. M. Zhong, JHEP 11 (2013) 167 [arXiv:1309.5084 [hep-ph]].
- [25] L. Darmé, S. A. R. Ellis, and T. You, JHEP 07 (2020) 053 [arXiv:2001.01490 [hep-ph]].
- [26] S. Schael *et al.* [ALEPH, DELPHI, L3, OPAL and LEP Electroweak Collaborations], Phys. Rept. 532 (2013) 119 [arXiv:1302.3415 [hep-ex]].
- [27] J. Abdallah *et al.* [DELPHI Collaboration], Eur. Phys. J. C 38 (2005) 395 [hep-ex/0406019]; J. Abdallah *et al.* [DELPHI Collaboration], Eur. Phys. J. C 60 (2009) 17 [arXiv:0901.4486 [hep-ex]].
- [28] B. Aubert *et al.* [BaBar Collaboration], [arXiv:0808.0017 [hep-ex]].
- [29] T. Abe *et al.* [Belle-II], [arXiv:1011.0352 [physics.ins-det]].
- [30] M. Aaboud *et al.* [ATLAS Collaboration], JHEP 1806 (2018) 166 [arXiv:1802.03388 [hep-ex]]; A. M. Sirunyan *et al.* [CMS Collaboration], Phys. Lett. B 792 (2019) 345 [arXiv:1808.03684 [hep-ex]].
- [31] [ATLAS Collaboration], ATLAS-CONF-2020-048.
- [32] [CMS Collaboration], Phys. Lett. B 792 (2019) 345 [arXiv:1808.03684 [hep-ex]].
- [33] O. Buchmueller, M. J. Dolan, S. A. Malik, and C. McCabe, JHEP 01 (2015) 037 [arXiv:1407.8257 [hep-ph]].
- [34] H. Zhang *et al.* [PandaX Collaboration], Science China (Phys. Mech. Astron.) 62 (2019) 31011, no.3 [arXiv:1806.02229 [physics.ins-det]].
- [35] D. Akerib *et al.* [LUX-ZEPLIN (LZ) Collaboration], Nucl. Instru. & Meth. A 953 (2020) 163047 [arXiv:1910.09124 [physics.ins-det]].
- [36] E. Aprile *et al.* [XENON Collaboration], JCAP 2011 (2020) 031 [arXiv:2007.08796 [physics.ins-det]]; JCAP 1604 (2016) 027 [arXiv:1512.07501 [physics.ins-det]].
- [37] For a review of the 2HDM, G. C. Branco, P. M. Ferreira, L. Lavoura, M. N. Rebelo, M. Sher and J. P. Silva, Phys. Rept. 516 (2012) 1 [arXiv:1106.0034 [hep-ph]]; and references therein.
- [38] T. P. Cheng and M. Sher, Phys. Rev. D 35 (1987) 3484
- [39] C. Alpigiani, A. Bevan, M. Bona, M. Ciuchini, D. Derkach, E. Franco, V. Lubicz, G. Martinelli, F. Parodi, and M. Pierini *et al.*, arXiv:1710.09644 [hep-ph].
- [40] G. Aad *et al.* [ATLAS Collaboration], Phys. Lett. B 801 (2020) 135148 [arXiv:1909.10235 [hep-ex]].